MODELS OF THE HEAT DYNAMICS OF SOLAR COLLECTORS FOR PERFORMANCE TESTING

Peder Bacher[1], Henrik Madsen[1] and Bengt Perers[2]

[1]DTU Informatics, Richard Pedersens Plads, Building 321, DK-2800 Lyngby, Denmark
[2]DTU Civil Engineering, Brovej, Building 118, DK-2800 Lyngby, Denmark

Abstract

The need for fast and accurate performance testing of solar collectors is increasing. This paper describes a new technique for performance testing which is based on non-linear continuous time models of the heat dynamics of the collector. It is shown that all important performance parameters can be accurately estimated with measurements from a single day. The estimated parameters are compared with results from standardized test methods (Fischer et al., 2004).

Modelling the dynamics of the collector is carried out using stochastic differential equations, which is a well proven efficient method to obtain accurate estimates of parameters in physical models. The applied method is described by Kristensen et al. (2004) and implemented in the software CTSM[1]. Examples of successful applications of the method includes modelling the of the heat dynamics of integrated photo-voltaic modules (Friling et al., 2009) and modelling of the heat dynamics of buildings (Madsen and Holst, 1995).

Measurements obtained at a test site in Denmark during the spring 2010 are used for the modelling. The tested collector is a single glazed large area flat plate collector with selective absorber and Teflon anti convection layer. The test rig is described in Fan et al. (2009).

The modelling technique provides uncertainty estimates such as confidence intervals for the parameters, and furthermore enables statistical validation of the results. Such tests can also facilitate procedures for selecting the best model to use, which is a very non-trivial task.

1 Introduction

This paper presents a new statistical approach for modelling the heat dynamics of a solar thermal collector. The applied modelling technique facilitates application of detailed models on data sampled with a relatively high sample rate. It is demonstrated that this allows for parameter estimation with high accuracy to be achieved with measurements from a single day. In the present study 2 seconds values averaged to 30 seconds values are used. Conventional non-dynamical models - by some called pseudo-dynamical models - of solar collectors cannot use such a high sample rate due to auto-correlation of the errors caused by non-modelled dynamical effects. The applied models are based on stochastic differential equations (SDEs), which gives the possibility to combine physical and data-driven statistical modelling. Such models are called grey-box models. A very strong feature of grey-box models is that they provide the possibility to estimate hidden state variables, i.e. variables in the model which are not measured. This allows using the same data for fitting models, with which the system is lumped differently, i.e. the physical model of the system can either be a single-state or a multi-state lumped model, which can be required for different types of collectors. Furthermore the modelling technique facilitates application of statistical tests to determine which model is most suitable for the given data. This is important for model identification and the approach is demonstrated in the paper. The modelling is carried out based on measurements from a period of 9 consecutive days in the beginning of May 2010. None of the days could have been used for stationary testing that is still the most common test method for solar collectors. Stationary testing requires perfect stable clear weather around noon. The measurements were performed on a single glazed large area flat plate collector with selective absorber and Teflon anti convection layer. The collector was not brand new, but has been in operation for 15 years, which affects the parameter values compared to todays products of the similar design. The results from the grey-box models are compared with results from the standardized EN 12975 Quasi Dynamic Test Method (CEN, European committee for standardization, 2006), which is based on multiple linear regression (MLR) modelling, to see if the estimation results matches current test standards. Finally, a thorough discussion and perspectives of the technique are given.

The paper is arranged as follows. The next section is a presentation of the theory of the applied grey-box models, with a simple example. This is followed by a section with a description of the MLR models used and thereafter a section with a description of all the considered grey-box models. Then the results are presented, and finally a discussion and perspective is given before the paper ends with a conclusion.

[1]`www2.imm.dtu.dk/~ctsm/`

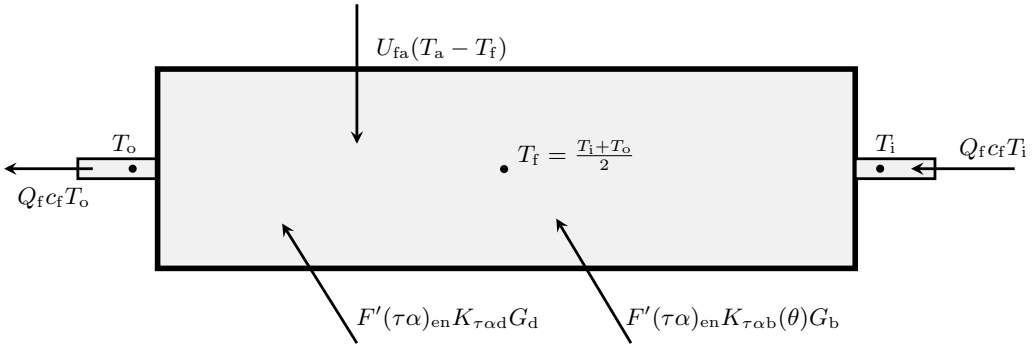

Figure 1: Diagram of *ToComp1* illustrating all the energy flows included in the model.

2 Grey-box models of a dynamic system

A grey-box model is established using a combination of prior physical knowledge and statistics, i.e. information embedded in data Kristensen et al. (2004). The prior physical knowledge is formulated by a set of non-linear stochastic differential equations (SDEs), also called a stochastic non-linear state-space model in continuous time. The equations describe a lumped model of the heat dynamics of the system.
The output of the solar collector is calculated by

$$q_{\mathrm{u}} = c_{\mathrm{f}}Q_{\mathrm{f}}(T_{\mathrm{o}} - T_{\mathrm{i}}) \tag{1}$$

where T_{o} is the outlet temperature and T_{i} is the inlet temperature. The output q_{u} is power output per square meter of collector aperture area and Q_{f} is flow per the same area. From Perers (1997) it is known that the output of a standard flat plate collector in first order accuracy level can be described by the heat balance

$$c_{\mathrm{f}}Q_{\mathrm{f}}(T_{\mathrm{o}} - T_{\mathrm{i}}) = F'(\tau\alpha)_{\mathrm{en}}K_{\tau\alpha\mathrm{b}}(\theta)G_{\mathrm{b}} + F'(\tau\alpha)_{\mathrm{en}}K_{\tau\alpha\mathrm{d}}G_{\mathrm{d}} - F'U_0(T_{\mathrm{f}} - T_{\mathrm{a}}) - (mC)_{\mathrm{e}}\frac{dT_{\mathrm{f}}}{dt} \tag{2}$$

For explanation of the symbols, see page 11. A linear temperature profile through the collector is applied by modelling the fluid temperature as a simple average

$$T_{\mathrm{f}} = \frac{T_{\mathrm{o}} + T_{\mathrm{i}}}{2} \tag{3}$$

The differential of the fluid temperature can then be written as

$$\frac{dT_{\mathrm{f}}}{dt} = \frac{1}{2}\frac{dT_{\mathrm{o}}}{dt} + \frac{1}{2}\frac{dT_{\mathrm{i}}}{dt} \tag{4}$$

which for a constant inlet temperature is

$$\frac{dT_{\mathrm{f}}}{dt} = \frac{1}{2}\frac{dT_{\mathrm{o}}}{dt} \tag{5}$$

This substitution, together with the addition of a noise term, is used to form the SDE

$$dT_{\mathrm{o}} = \Big(F'U_0(T_{\mathrm{a}} - T_{\mathrm{f}})dt + c_{\mathrm{f}}Q_{\mathrm{f}}(T_{\mathrm{i}} - T_{\mathrm{o}})dt + F'(\tau\alpha)_{\mathrm{en}}K_{\tau\alpha\mathrm{b}}(\theta)G_{\mathrm{b}}dt + F'(\tau\alpha)_{\mathrm{en}}K_{\tau\alpha\mathrm{d}}G_{\mathrm{d}}dt\Big)\frac{2}{(mC)_{\mathrm{e}}} + \sigma d\omega \tag{6}$$

which describes the heat dynamics for the collector in the simplest grey-box model considered in the paper. It is denoted as *ToComp1*. In grey-box terminology this is called the system equation of the state-space model. The noise term $\sigma d\omega$ is called the system noise and consist of increments of $\{\omega\}$, which is a standard Wiener process, and σ^2, which is the incremental variance of the Wiener process. In this model the collector is lumped into one single part and the state variable is the outlet temperature T_{o}. An illustration of the model is found in Figure 1.

The physical model part is coupled with the data-driven model part with which the information embedded in observed data is used for parameter estimation. The data-driven part in the considered example is represented by the discrete time measurement equation

$$Y_k = T_{ok} + e_k \tag{7}$$

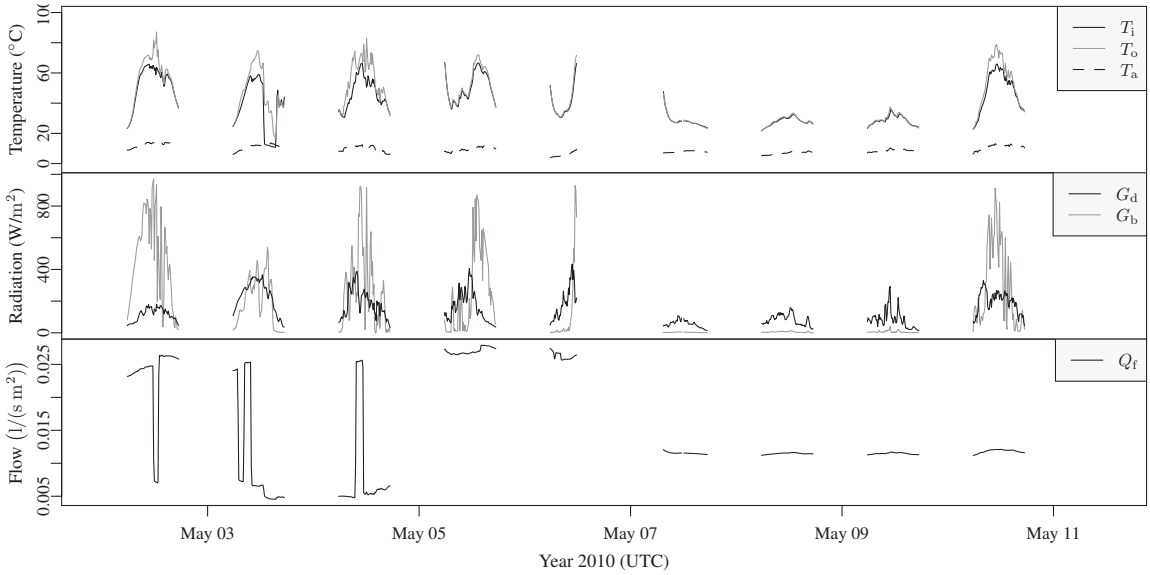

Figure 2: The data as 10 minutes averaged values. The upper plot is the measured temperatures, the middle plot is the diffuse and direct (beam) radiation, and the lowest plot is the fluid flow.

where k is the point in time t_k of a measurement, Y_k is the measured outlet temperature, and e_k is the measurement error, which is assumed to be a Gaussian white noise process with variance σ^2. This assumption - plus the assumption that W is a Wiener process - enables evaluation and tests of the performance of the model, since such tests can show if the physical model is consistent with the observed heat dynamics of the collector.

2.1 Maximum likelihood estimation of parameters

Given a grey-box model, as described above, maximum likelihood estimates of the parameters can be obtained. Let the N observations be represented by

$$\mathcal{Y}_N = [Y_N, Y_{N-1}, \ldots, Y_1, Y_0] \tag{8}$$

then the likelihood function is the joint probability density

$$L(\theta; \mathcal{Y}_N) = \left(\prod_{k=1}^{N} p(Y_k | \mathcal{Y}_{k-1}, \theta) \right) p(Y_0 | \theta) \tag{9}$$

where $p(Y_k|\mathcal{Y}_{k-1}, \theta)$ is a conditional density denoting the probability of observing Y_k given the previous observations and the parameters θ, and where $p(Y_0|\theta)$ is a parameterization of the starting conditions Kristensen et al. (2004). The maximum likelihood estimates of the parameters are then found by

$$\hat{\theta} = \arg\max_{\theta} \left\{ L(\theta; \mathcal{Y}_N) \right\} \tag{10}$$

Due to the previously mentioned assumptions about the system and measurement noise, it follows that the conditional densities in Equation (10) can be well approximated by Gaussian densities. Hence an extended Kalman filter can be used to calculate the likelihood function, and an optimization algorithm can be applied to maximize it, thereby calculating the maximum likelihood estimates, see Kristensen et al. (2004) for a detailed discussion. This is implemented in the computer software CTSM, which has been used for carrying out the parameter estimation. See more about the methods and software at [2] and in Kristensen and Madsen (2003).

3 Experimental setup and data

The experiments are described by Fan et al. (2009) and were carried out in the spring of 2010. The measurements were obtained with a 2 seconds sample interval. For the present study models are identified for both 30

[2] `www.imm.dtu.dk/~ctsm`

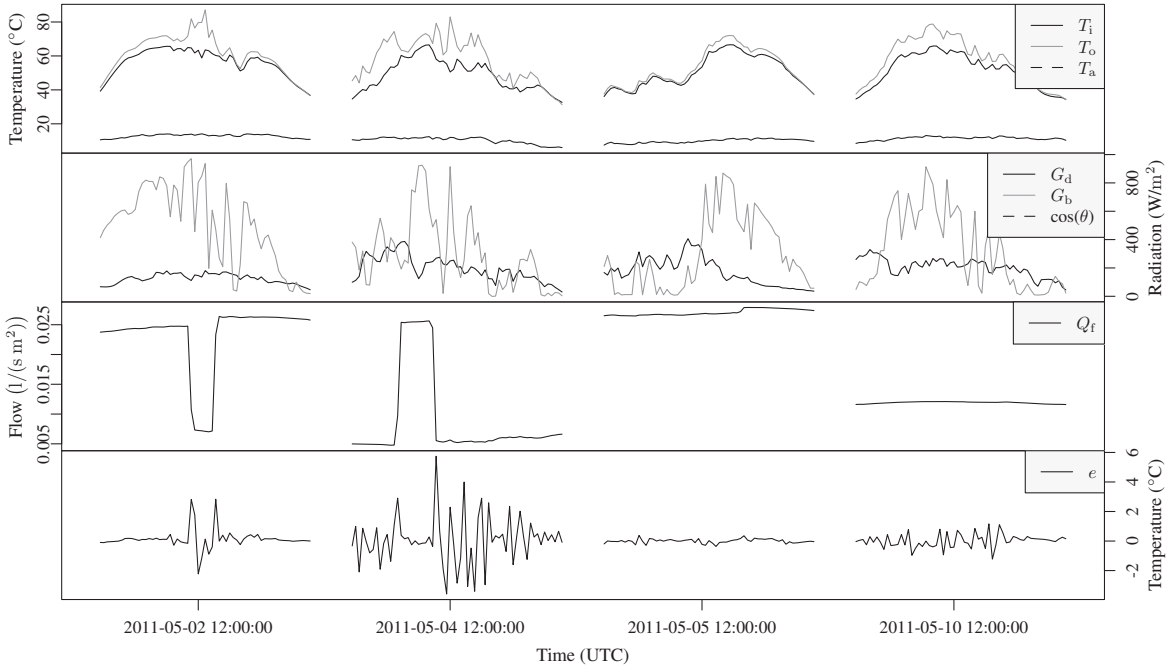

Figure 3: The 10 minutes averaged values from days where the model *ToComp1* is fitted. The upper plot is of the inlet-, outlet-, and the ambient temperature. Below this is shown a plot of the direct- and diffuse solar radiation, followed by a plot of the fluid flow. The lowest plot is the residuals from the fit from each day, this is referred to in a later in the paper.

seconds and 10 minutes average values. The data resampled to 10 minute average values is plotted in Figure 2. Only time points where the angle of incidence is lower than 84 degrees are used. For the parameter estimation it is important to acquire a period, for which the input signals are as uncorrelated as possible and cover the typical range of operation. Periods with full cloud cover are not feasible, since there is not enough variation in the direct radiation and in periods with no cloud cover the radiation and the module temperature is highly correlated. Hence days with varying cloud cover are most appropriate and these days are the most common in most locations where people traditionally live.

4 Multiple linear regression models

The EN 12975 Quasi Dynamic Test Method (CEN, European committee for standardization, 2006) is applied to have a reference for the results from the new proposed method. The method is based on multiple linear regression (MLR) modelling, where down to 5 minutes average values are recommended. The data was re-sampled to 10 minutes averages, which for all 9 days gives 593 time points. MLR modelling with 5 minutes averages was tried and the results were only marginally different. The following model structure is applied

$$q_t^{\mathrm{u}} = F'(\tau\alpha)_{\mathrm{en}} K_{\tau\alpha\mathrm{b}}(\theta) G_t^{\mathrm{b}} + F'(\tau\alpha)_{\mathrm{en}} K_{\tau\alpha\mathrm{d}} G_t^{\mathrm{d}} + F'U_0 \Delta T_t + F'U_1 \Delta T_t^2 - F'U_{\mathrm{w}} \Delta T_t w_t - (mC)_{\mathrm{e}} \frac{dT_t^{\mathrm{f}}}{dt} + e_t \tag{11}$$

where $\Delta T_t = T_t^{\mathrm{a}} - T_t^{\mathrm{f}}$. Three models are fitted: *MLR1* without $F'U_1$ and $F'U_{\mathrm{w}}$, *MLR2* without $F'U_1$, and *MLR3* with all inputs.

5 Applied grey-box models

This section gives an overview of the applied grey-box models and the parts of the data on which the parameter estimation was carried out. First the single state grey-box model *ToComp1*, described in Section 2 was fitted to 10 minutes average values on the days with varying cloud cover. This data is plotted in Figure 3. The model was fitted to each day separately and finally to all four days pooled together. In addition to the *ToComp1* model four other grey-box models have been fitted to the data from the 10'th of May resampled to 30 second average values. This gives $N = 1413$ data points, which are plotted in Figure 4. The additional four models are expanded as more detailed versions of *ToComp1*. There are two ways to expand the model: either more inputs

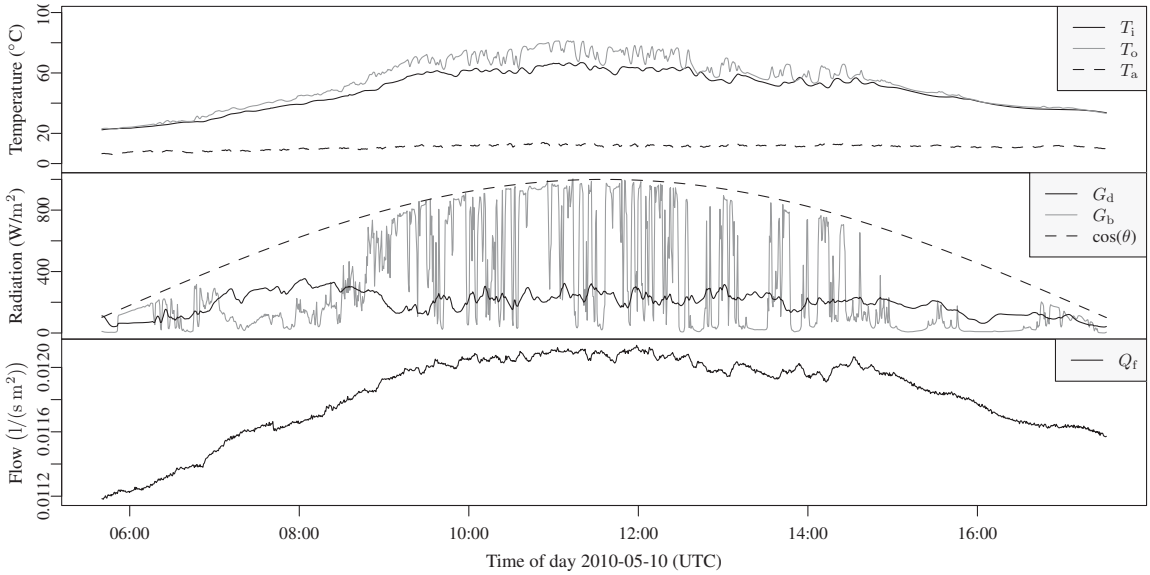

Figure 4: The 30 seconds averaged data for which the modelling is applied. The upper plot is of the inlet-, outlet-, and the ambient temperature. Below this is a plot of the direct- and diffuse solar radiation, followed by the plot of the fluid flow.

(explanatory variables) can be used, or - since the models are lumped models - a better representation can maybe be achieved by lumping the system into more parts (also called compartments, states, zones, or nodes). The latter approach is considered in the following. The first two expanded models are made more detailed by lumping the collector into more than one compartment in the flow direction of the collector fluid, such that the temperature of the collector is represented by two or more temperature state variables. This allows for a better representation of the temperature differences between the inlet - the cold side when solar radiation level is high - and the outlet of the collector. Furthermore this also gives a better description of the delay introduced since it takes time for the fluid to flow through the collector. For the current setup and the flow of the 10'th of May, this is around 1 minute. These two models are denoted by *ToComp2* and *ToComp3*. The third expanded model is denoted by *ToTmComp1* and in this model the collector is lumped in two parts: one representing the fluid and one representing the solid part of the collector. This is a better description of the system, in which the solar radiation first heats up the collector which then heats up the fluid. Finally, the fourth expanded model *TmToComp2* is a combination of the two approaches, where the collector is first divided in two parts - one for the fluid and one for the collector - which then each are divided into two compartments in the flow direction of the fluid.

5.1 Models with multiple compartments in the flow direction

The *ToComp1* model can be expanded to a n_c compartment model with the system equations

$$\begin{aligned}
dT_{\mathrm{o}1} &= \Big(F'U_0(T_\mathrm{a}-T_{\mathrm{f}1})+n_\mathrm{c}c_\mathrm{f}Q_\mathrm{f}(T_\mathrm{i}-T_{\mathrm{o}1})+F'(\tau\alpha)_\mathrm{en}K_{\tau\alpha\mathrm{b}}(\theta)G_\mathrm{b}+F'(\tau\alpha)_\mathrm{en}K_{\tau\alpha\mathrm{d}}G_\mathrm{d}\Big)\frac{2}{(mC)_\mathrm{e}}dt+\sigma_1 d\omega_1 \\
dT_{\mathrm{o}2} &= \Big(F'U_0(T_\mathrm{a}-T_{\mathrm{f}2})+n_\mathrm{c}c_\mathrm{f}Q_\mathrm{f}(T_{\mathrm{o}1}-T_{\mathrm{o}2})+F'(\tau\alpha)_\mathrm{en}K_{\tau\alpha\mathrm{b}}(\theta)G_\mathrm{b}+F'(\tau\alpha)_\mathrm{en}K_{\tau\alpha\mathrm{d}}G_\mathrm{d}\Big)\frac{2}{(mC)_\mathrm{e}}dt+\sigma_2 d\omega_2 \\
&\vdots \\
dT_{on_\mathrm{c}} &= \Big(F'U_0(T_\mathrm{a}-T_{\mathrm{f}n_\mathrm{c}})+n_\mathrm{c}c_\mathrm{f}Q_\mathrm{f}(T_{\mathrm{o}(n_\mathrm{c}-1)}-T_{on_\mathrm{c}})+F'(\tau\alpha)_\mathrm{en}K_{\tau\alpha\mathrm{b}}(\theta)G_\mathrm{b}+F'(\tau\alpha)_\mathrm{en}K_{\tau\alpha\mathrm{d}}G_\mathrm{d}\Big)\frac{2}{(mC)_\mathrm{e}}dt+\sigma_2 d\omega_2
\end{aligned} \tag{12}$$

where n_c is the number of compartments. The accompanying measurement equation is

$$Y_k = T_{on_\mathrm{c}k}+e_k \tag{13}$$

Two models of this type are fitted to the data: *ToComp2* with two compartments, and *ToComp3* with three compartments. A diagram illustrating *ToComp2* is shown in Figure 5

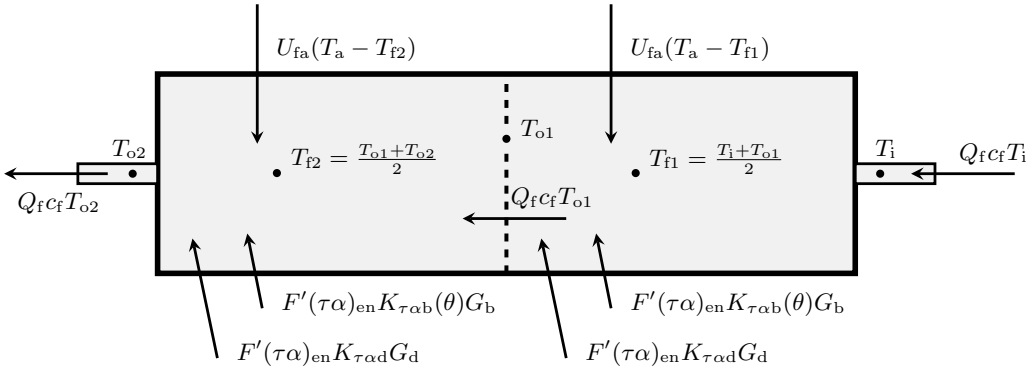

Figure 5: The *ToComp2* model with two compartments in the flow direction of the fluid.

5.2 Models divided into a collector and a fluid part

The *TmToComp1* model illustrated in Figure 6, where the panel is divided into two parts, has the system equation

$$dT_{\mathrm{m}} = \Big(F'(\tau\alpha)_{\mathrm{en}}K_{\tau\alpha\mathrm{b}}(\theta)G_{\mathrm{b}} + F'(\tau\alpha)_{\mathrm{en}}K_{\tau\alpha\mathrm{d}}G_{\mathrm{d}} + U_{\mathrm{fm}}(T_{\mathrm{f}} - T_{\mathrm{m}}) + U_{\mathrm{ma}}(T_{\mathrm{a}} - T_{\mathrm{m}})\Big)\frac{1}{(mC)_{\mathrm{e}}}dt + \sigma_m d\omega_m \tag{14}$$

$$dT_{\mathrm{o}} = \Big(U_{\mathrm{fm}}(T_{\mathrm{m}} - T_{\mathrm{f}}) + c_{\mathrm{f}}Q_{\mathrm{f}}(T_{\mathrm{i}} - T_{\mathrm{o}})\Big)\frac{2}{(mC)_{\mathrm{e}}}dt + \sigma_o d\omega_o$$

It is seen that the solar radiation enters the collector part, which then heats up the fluid by conduction. Of the considered models the most detailed model is *TmToComp2*, in which the collector is both divided into two parts and 2 compartments in the fluid flow direction for each part. The following system equations is formulated for a model with two parts having each n_{c} compartments

$$\begin{aligned}
dT_{\mathrm{m1}} &= \Big(F'(\tau\alpha)_{\mathrm{en}}K_{\tau\alpha\mathrm{b}}(\theta)G_{\mathrm{b}} + F'(\tau\alpha)_{\mathrm{en}}K_{\tau\alpha\mathrm{d}}G_{\mathrm{d}} + U_{\mathrm{fm}}(T_{\mathrm{f1}} - T_{\mathrm{m1}}) + U_{\mathrm{ma}}(T_{\mathrm{a}} - T_{\mathrm{m1}})\Big)\frac{1}{(mC)_{\mathrm{e}}}dt + \sigma_{\mathrm{m1}}d\omega_{\mathrm{m1}} \\
dT_{\mathrm{o1}} &= \Big(U_{\mathrm{fm}}(T_{\mathrm{m1}} - T_{\mathrm{f1}}) + n_{\mathrm{c}}c_{\mathrm{f}}Q_{\mathrm{f}}(T_{\mathrm{i}} - T_{\mathrm{o1}})\Big)\frac{2}{(mC)_{\mathrm{e}}}dt + \sigma_{\mathrm{o1}}d\omega_{\mathrm{o1}} \\
dT_{\mathrm{m2}} &= \Big(F'(\tau\alpha)_{\mathrm{en}}K_{\tau\alpha\mathrm{b}}(\theta)G_{\mathrm{b}} + F'(\tau\alpha)_{\mathrm{en}}K_{\tau\alpha\mathrm{d}}G_{\mathrm{d}} + U_{\mathrm{fm}}(T_{\mathrm{f2}} - T_{\mathrm{m2}}) + U_{\mathrm{ma}}(T_{\mathrm{a}} - T_{\mathrm{m2}})\Big)\frac{1}{(mC)_{\mathrm{e}}}dt + \sigma_{\mathrm{m2}}d\omega_{\mathrm{m2}} \\
dT_{\mathrm{o2}} &= \Big(U_{\mathrm{fm}}(T_{\mathrm{m2}} - T_{\mathrm{f2}}) + n_{\mathrm{c}}c_{\mathrm{f}}Q_{\mathrm{f}}(T_{\mathrm{o1}} - T_{\mathrm{o2}})\Big)\frac{2}{(mC)_{\mathrm{e}}}dt + \sigma_{\mathrm{o2}}d\omega_{\mathrm{o2}} \\
&\vdots \\
dT_{\mathrm{m}n_{\mathrm{c}}} &= \Big(F'(\tau\alpha)_{\mathrm{en}}K_{\tau\alpha\mathrm{b}}(\theta)G_{\mathrm{b}} + F'(\tau\alpha)_{\mathrm{en}}K_{\tau\alpha\mathrm{d}}G_{\mathrm{d}} + U_{\mathrm{fm}}(T_{\mathrm{f}n_{\mathrm{c}}} - T_{\mathrm{m}n_{\mathrm{c}}}) + U_{\mathrm{ma}}(T_{\mathrm{a}} - T_{\mathrm{m}n_{\mathrm{c}}})\Big)\frac{1}{(mC)_{\mathrm{e}}}dt + \sigma_{\mathrm{m}n_{\mathrm{c}}}d\omega_{\mathrm{m}n_{\mathrm{c}}} \\
dT_{\mathrm{o}n_{\mathrm{c}}} &= \Big(U_{\mathrm{fm}}(T_{\mathrm{m}n_{\mathrm{c}}} - T_{\mathrm{f}n_{\mathrm{c}}}) + n_{\mathrm{c}}c_{\mathrm{f}}Q_{\mathrm{f}}(T_{\mathrm{o1}} - T_{\mathrm{o}n_{\mathrm{c}}})\Big)\frac{2}{(mC)_{\mathrm{e}}}dt + \sigma_{\mathrm{o}n_{\mathrm{c}}}d\omega_{\mathrm{o}n_{\mathrm{c}}}
\end{aligned} \tag{15}$$

i.e. the *TmToComp2* model has $n_{\mathrm{c}} = 2$.

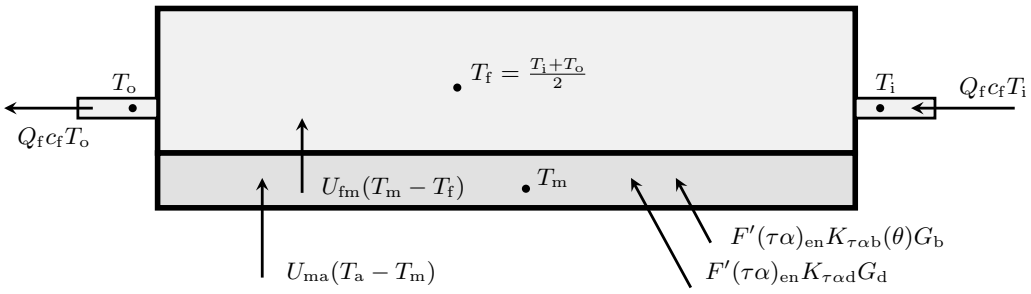

Figure 6: Diagram illustrating the *TmToComp1* model. The collector is divided into a part representing the fluid and another part representing the collector.

Table 1: Parameter estimates with MLR models. The standard deviation of the estimate is in parenthesis to the right of the estimated value. Insignificant terms are marked with *.

Parameter	*MLR1*		*MLR2*		*MLR3*		Units
$F'(\tau\alpha)_{\mathrm{en}}$	0.737	(0.0031)	0.741	(0.0030)	0.746	(0.0043)	
b_0	0.166		0.172		0.175		
$K_{\tau\alpha\mathrm{d}}$	0.891		0.904		0.895		
$F'U_0$	2.18	(0.45)	2.13	(0.045)	2.02	(0.082)	$[\mathrm{W}/(\mathrm{m}^2\mathrm{K})]$
$F'U_1$					0.0031*	(0.0020)	$[\mathrm{W}/(\mathrm{m}^2\mathrm{K})]$
$F'U_{\mathrm{w}}$			0.192	(0.034)	0.179	(0.035)	$[\mathrm{W}/(\mathrm{m}^2\mathrm{K})]$
$(mC)_{\mathrm{e}}$	4699	(130)	4751	(127)	4788	(129)	$[\mathrm{J}/(\mathrm{m}^2\mathrm{K})]$

6 Results

In this section the results of the parameter estimation with the described models are presented. Firstly, the results from the traditional MLR models fitted on the entire data set of 10 minutes values is presented, secondly from grey-box model *ToComp1* fitted on individual days of 10 minutes values, and finally all grey-box models fitted on 30 seconds values from the 10'th of May. The parameter estimates together with the their standard deviation are presented in tables, and time series of the residuals together with other relevant error measures are plotted. A short outline of the model identification carried out is also provided.

6.1 MLR models

The parameter estimates are listed in Table 1. The estimates are clearly within the typical range for this type of collector, see Perers (1993) and Solar Keymark homepage (Solar Keymark, 2011). The collector under test has been in operation for 15 years, this affects the parameter values compared to todays products. The standard deviations show that the parameters are very accurately determined. The only non-significant term are $F'U_1$ in *MLR3*, which leads the conclusion that *MLR2* is the most appropriate model of the three. For evaluation of the model fit the measured collector output versus the predicted is plotted in Figure 7. It is seen that the measured output is predicted very well, although it does seems like the variance increase slightly with the output. This is most likely due to the periods with low flow rate for some of the days. Furthermore the inlet temperature variation range is not fully as high as specified in the standard for the selected days.

6.2 ToComp1 fitted to 10 minutes values

The single state grey-box model defined in Equation (6) is fitted to both 10 minutes values from four separate days and all four pooled together. The estimated parameter are listed in Table 2. Clearly the parameter estimates matches the estimates from the MLR models quite well considering the standard deviations, especially the parameters $F'(\tau\alpha)_{\mathrm{en}}$ and $F'U_0$, which are the most important parameters for evaluation of the collector performance. A very apparent deviation of the results between the days is that the lowest uncertainty is found on the 5'th of May. This is not a surprise considering a plot of the residuals, which is shown in the lowest plot

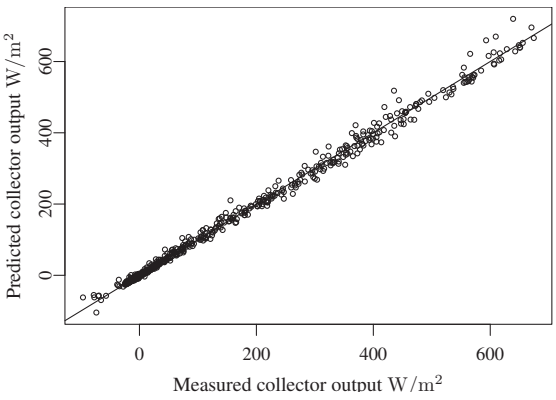

Figure 7: Measured versus the predicted collector output from *MLR2*.

Table 2: Parameter estimates from *ToComp1* fitted to 10 minutes values from single days and all four days pooled. The standard deviation is given in parenthesis to the right of the estimate.

	2011-05-02		2011-05-04		2011-05-05		2011-05-10		Pooled	
$F'(\tau\alpha)_{\mathrm{en}}$	0.755	(0.032)	0.785	(0.032)	0.746	(0.0086)	0.758	(0.014)	0.763	(0.011)
b_0	0.204	(0.039)	0.201	(0.046)	0.18	(0.017)	0.182	(0.023)	0.195	(0.020)
$K_{\tau\alpha\mathrm{d}}$	0.903	(0.42)	0.857	(0.11)	0.819	(0.027)	0.867	(0.049)	0.839	(0.034)
$F'U_0$	2.07	(1.1)	2.4	(0.35)	1.73	(0.13)	2.16	(0.26)	2.05	(0.18)
$(mC)_{\mathrm{e}}$	6050	(1060)	6200	(1130)	5040	(279)	5020	(92)	5666	(638)

Table 3: The parameter estimates from the grey-box models fitted to 30 seconds values from the 10'th of May. Note that the parameters represent different physical entities from the three first model (prefixed with *To*) to the last two models (prefixed with *TmTo*) and therefore cannot be directly compared. For each estimate the standard deviation is given in parenthesis to the right of the estimate.

	ToComp1		ToComp2		ToComp3		TmToComp1		TmToComp2	
$F'(\tau\alpha)_{\mathrm{en}}$	0.767	(0.0036)	0.751	(0.0027)	0.743	(0.0015)	0.816	(0.0025)	0.792	(0.00096)
b_0	0.172	(0.0063)	0.177	(0.0017)	0.18	(0.00044)	0.188	(0.0038)	0.189	(0.00067)
$K_{\tau\alpha\mathrm{d}}$	0.942	(0.015)	0.933	(0.0042)	0.931	(0.002)	0.929	(0.008)	0.927	(0.0021)
U_{fa}	2.55	(0.076)	2.31	(0.049)	2.2	(0.023)				
U_{fm}							49.8	(2.5)	83.7	(0.83)
U_{ma}							2.37	(0.042)	2.22	(0.016)
C_{f}	6960	(80)	8020	(17)	8580	(36)	3750	(114)	3390	(54)
C_{m}							962	(64)	1690	(22)

of Figure 3. The level of the residuals from the fit to this day are smaller than for the other days, and this is apparently due to the level of the fluid flow, which is plotted above the residuals in the figure. The parameter estimates based on the four days pooled together seems like a compromise between the estimates from the single days.

6.3 Grey-box models fitted to 30 seconds values

The five grey-box models described are fitted to the data from the 10'th of May resampled to 30 seconds averages. The parameter estimates are listed in Table 3. First, it is noticed that the parameters of the three models prefixed with *To* are not representing the same physical entities as they do in the models prefixed with *ToTm*, since the collector is lumped differently in the models. The increase of the value of $F'(\tau\alpha)_{\mathrm{en}}$ from *To* to *ToTm* models is found to be consistent with the physical representation, since the reference temperature is closer to the absorber surface. This means that the estimated optical parameter for the *ToTm* models is rather $\tau\alpha$. The value F' is in the range of 0.95 for this collector design, which leads to an estimate of $F'(\tau\alpha)_{\mathrm{en}}$ to 0.752 for *ToTmComp2*.

Plots of the residual series from each model are shown in Figure 8. Clearly the level of the residuals decrease from the upper to the lower plot and the highest errors occur when a cloud passes by and the level of direct solar radiation shifts rapidly. The decreased level of the variation of the residuals indicates that the more detailed models are better. To verify this, statistical likelihood-ratio tests is applied as described by Bacher and Madsen (2011). The log-likelihood of the fit for each model is listed in Table 4, together with the number of parameters, and the p-value of tests for model expansion. The tests for expansion is a model versus the expanded model a single step to the right in the table, except for *nl2TmToComp1*, from which the expansion is from *nl2ToComp2*. The results of the tests are very clear, all expansions are significant. Hence it is concluded that *nl2TmToComp2* is the most suitable model of these five models and that it might very well be, that the model could be further expanded. Finally, the auto-correlation function (ACF) and the cumulated periodogram (CP) Madsen (2007) of the residuals are shown in Figure 9. The dashed blue lines indicate 95% confidence intervals for a white noise. According to theory, presented in Section 2, then if the residual series are white noise this indicates that the grey-box model is consistent with the observed heat dynamics of the collector. From the ACF and CP it is seen that the residuals are close to having white noise properties. Interestingly it is seen that residuals from *ToComp1* are more white noise like than the residuals from *TmToComp1*. It is found that this is caused by a low signal to noise ratio in the residuals for *ToTmComp1*, i.e. the dominating errors are on a high frequency which have characteristics like white noise. As the detailed models includes the faster

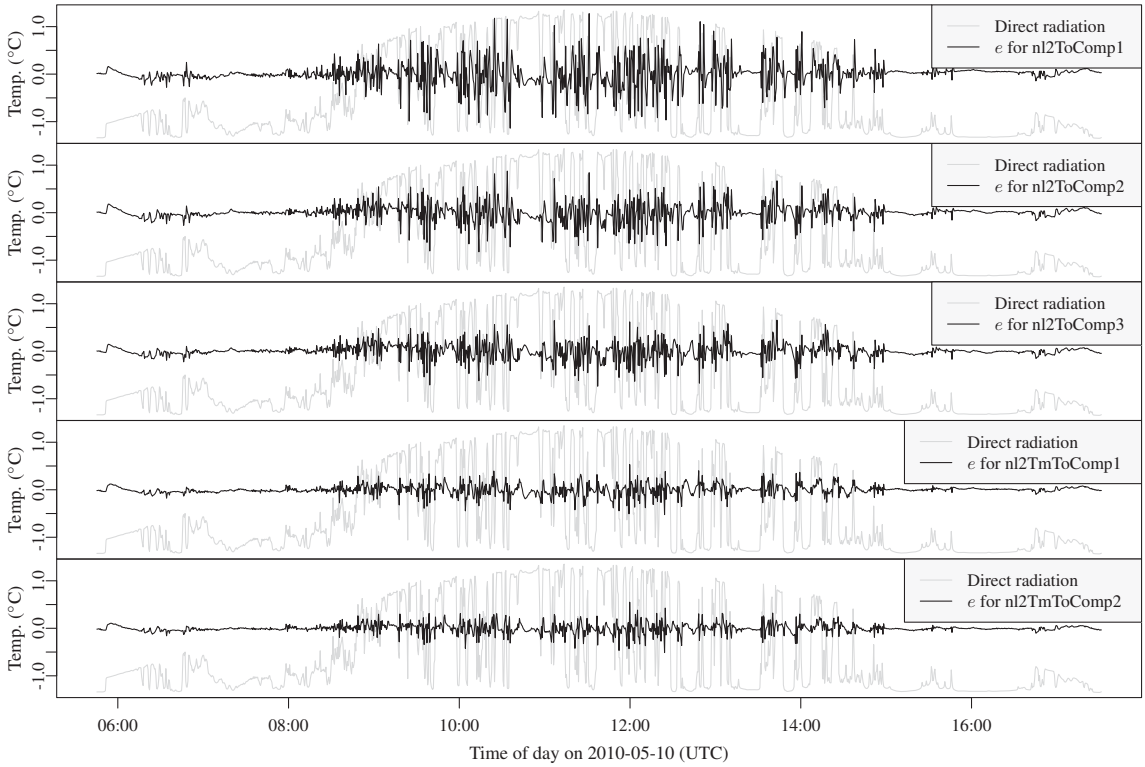

Figure 8: The residual series from the grey-box models fitted to 30 seconds values from the 10'th of May. The greyed series are the direct solar radiation.

dynamics, the high frequency errors are decreased, and they do not "hide" the remaining signal components in the residuals. However for the most detailed model almost all the systematic variation in the data is described.

7 Discussion and applications

In general the results from the MLR models and the grey-box are found to match well, but it is noted that the result the from grey-box model *ToComp1* fitted on separate days - which have different conditions, especially in the fluid flow level - gives some variation to the estimates. Therefore it is concluded that attention has to be put on the experimental design in order to ensure stable and accurate parameter estimation for collector testing with grey-box models. Regarding the more detailed grey-box models fitted to 30 seconds values, it is found that since the likelihood is not saturated, i.e. the likelihood-ratio tests are very significant, further expansion of the *TmToComp2* is still possible. From the plots of the residuals in Figure 8, it is seen that the error level certainly is highest just after the direct radiation shifts its level very rapidly, and it is this effect that seems to be improved as the more detailed models are used. Hence the main improvement from the one-state model *ToComp1* to the multi-state models are in the description of the fast dynamics, which includes the delay caused by movement of the fluid through the collector, e.g. when the direct radiation shifts from a high to a low level, the fluid passing out of the collector are still hot for some time. This also indicates the importance of the experiment design, since for dynamic condition the frequency, with which the system is excited, affect which grey-box model is optimal. For example if the direct radiation varies with a lower frequency, a simpler model might be in favour over more complex models, whereas for variation with a higher frequency the inclusion of the fast dynamics

Table 4: Log-likelihood, number of parameters, and p-value of likelihood-ratio tests for model expansion for each of the grey-box models.

	nl2ToComp1	nl2ToComp2	nl2ToComp3	nl2TmToComp1	nl2TmToComp2
Log-likelihood	-35.51	454.8	661	1185	1307
Number of prm.	9	12	14	13	18
p-value		≈ 0	≈ 0	≈ 0	≈ 0

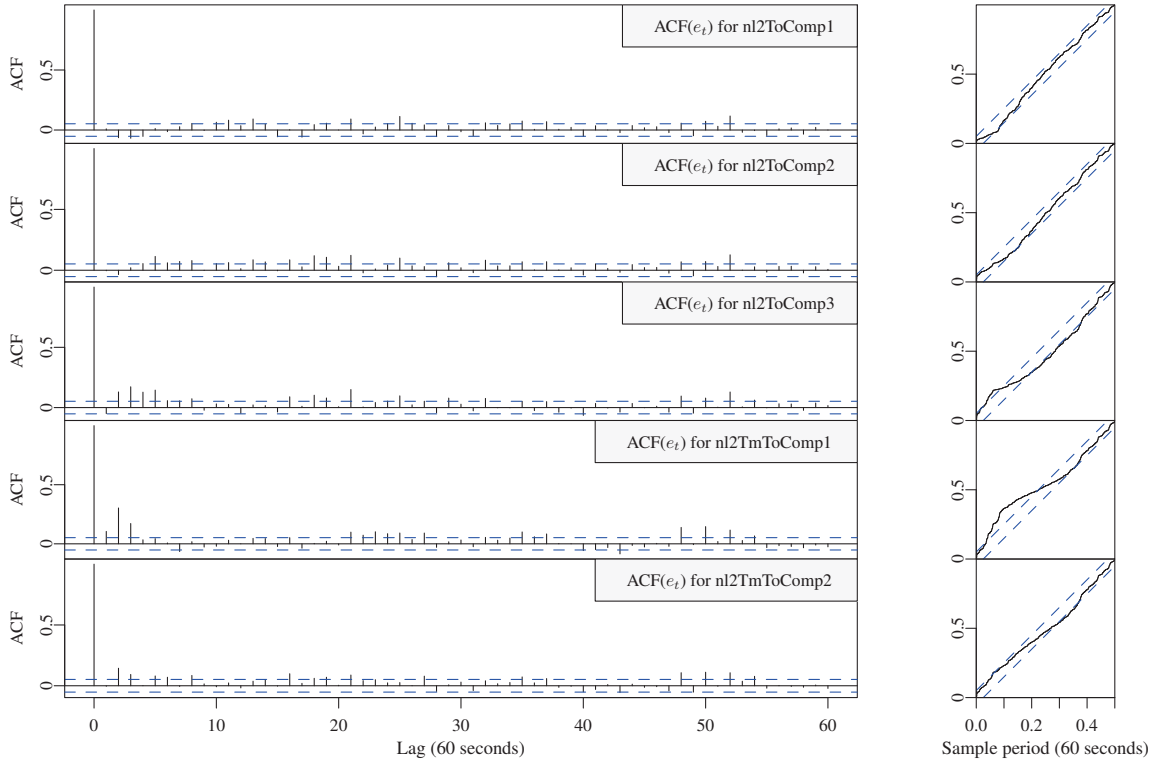

Figure 9: Plots of the auto-correlation function (ACF) and the cumulated periodogram of the residuals from each of the grey-box models fitted on 30 seconds values.

are more important. Therefore if the main excitation of the system, i.e. the direct radiation, can be controlled, it will be possible to achieve fast and accurate parameter estimation. This could be carried out with a simple shadowing device, which should be controlled with PRBS signal to gain maximum information of the heat dynamics of the system (Madsen and Holst, 1995). Higher accuracy can also be achieved with more systematic variation of the inlet temperature, this also applies for the MLR modelling. The right experiment design will allow inclusion of night measurements - which will improve the separation of heat loss and radiation effects and thereby more accurate estimation - and furthermore allow for inclusion of more effects, such as wind and non-linear radiation effects between the collector and the surroundings. Finally, dividing the collector into more parts, e.g. one representing the fluid, one representing the metal, and one representing the surrounding collector body could be tried.

7.1 Applications

The most apparent application of grey-box modelling of the heat dynamics of solar collectors are for the development of fast and accurate performance testing, especially for some types of collectors multi-state models are needed to obtain a required level of accuracy. Especially vacuum tube collectors of dewar type can have an extra time delay due to the high thermal resistance between the heat transfer fluid and absorber surface that is not fully taken up by the present collector model used for performance testing. The new approach described here, particularly with the *TmTo* models, has the potential to deal with this in an accurate way. Additional applications include optimization of operation with model predictive control, which the grey-box models are perfectly suited for. Especially larger solar thermal plants might be able to gain much in performance by applying grey-box modelling and model predictive control.

8 Conclusion

Successful modelling of a the heat dynamics of a solar collector with grey-box models has been carried out. The results have been compared to the EN-standard MLR modelling and they are in agreement. It is shown that high accuracy parameter estimates was obtained with measurements from a single day resampled to 30 seconds average values. This will enable lowering of testing time significantly compared to current test methods.

Highly detailed models of the heat dynamics of the solar collector can be applied, which can be useful for many types of collectors. It is found that the conditions under which the experiment was carried out influence the parameter estimates. Therefore it is concluded that experiment design is the key to achievement of fast, reliable and high accuracy collector testing methods with grey-box models. Experiments with PRBS variation of direct radiation with shadowing device should be carried out to obtain higher accuracy and reproducibility of the results, and finally models with more explanatory variables, such as wind and long-wave radiation should be further elaborated.

Nomenclature

The same notation as in Perers (1997) are used as widely as possible.

Collector model parameters:

$F'(\tau\alpha)_{\mathrm{en}}$	Zero loss efficiency for direct radiation at normal incidence
$K_{\tau\alpha\mathrm{b}}(\theta)$	Incidence angle modifier for direct radiation
$K_{\tau\alpha\mathrm{d}}$	Incidence angle modifier for diffuse radiation
$F'U_0$	Heat loss coefficient at $(T_{\mathrm{a}} - T_{\mathrm{f}}) = 0$, $\left[\mathrm{W}/(\mathrm{m}^2\mathrm{K})\right]$.
$F'U_1$	Temperature dependence of the heat loss coefficient, $\left[\mathrm{W}/(\mathrm{m}^2\mathrm{K}^2)\right]$.
$F'U_{\mathrm{w}}$	Wind dependence of the heat loss coefficient, $\left[\mathrm{Ws}/(\mathrm{m}^3\mathrm{K})\right]$.
$(mC)_{\mathrm{e}}$	Effective thermal capacitance including piping for the collector, $\left[\mathrm{J}/(\mathrm{m}^2\mathrm{K})\right]$.
C_{f}	Fluid thermal capacitance, $\left[\mathrm{J}/(\mathrm{m}^2\mathrm{K})\right]$.
C_{m}	Collector thermal capacitance, $\left[\mathrm{J}/(\mathrm{m}^2\mathrm{K})\right]$.
U_{fa}	Heat transmission coefficient from fluid to ambient, $\left[\mathrm{J}/(\mathrm{Km}^2)\right]$.
U_{fm}	heat transmission coefficient from fluid to module, $\left[\mathrm{J}/(\mathrm{Km}^2)\right]$.
U_{ma}	heat transmission coefficient from module to ambient, $\left[\mathrm{J}/(\mathrm{Km}^2)\right]$.
n_{c}	Number of compartments

Measured variables:

G_{d}	Diffuse radiation onto the collector plane, $\left[\mathrm{W}/\mathrm{m}^2\right]$.
G_{b}	Direct radiation onto the collector plane, $\left[\mathrm{W}/\mathrm{m}^2\right]$.
T_{a}	Ambient air temperature near the collector, $[^\circ\mathrm{C}]$.
T_{o}	Outlet temperature of the collector, $[^\circ\mathrm{C}]$.
T_{i}	Temperature of the inlet to the collector, $[^\circ\mathrm{C}]$.
Q_{f}	Flow of the fluid per square meter of collector, $\left[\mathrm{l}/(\mathrm{sm}^2)\right]$.
θ	incidence angle for the direct solar radiation onto the collector plane, $[\mathrm{radians}]$.
w	Wind speed, $[\mathrm{m}/\mathrm{s}]$.

Derived variables etc.:

T_{f}	Average temperature of the collector fluid, $[^\circ\mathrm{C}]$.
T_{m}	Average temperature of the collector, $[^\circ\mathrm{C}]$.
q_{u}	Collector power output, $\left[\mathrm{W}/\mathrm{m}^2\right]$.
c_{f}	Specific heat capacity of the fluid, $[\mathrm{J}/(\mathrm{lK})]$.

References

P. Bacher and H. Madsen. Identifying suitable models for the heat dynamics of buildings. *Energy & Buildings*, 43(7): 1511–1522, 2011. ISSN 03787788. doi: 10.1016/j.enbuild.2011.02.005.

CEN, European committee for standardization. En 12975-2:2006, thermal solar systems and components - collectors - part 2: Test methods, 2006.

J. Fan, Z. Chen, S. Furbo, B. Perers, and B. Karlsson. Efficiency and lifetime of solar collectors for solar heating plants. Proceedings of the ISES Solar World Congress 2009: Renewable Energy Shaping Our Future, 2009.

S. Fischer, W. Heidemann, H. Müller-Steinhagen, B. Perers, P. Bergquist, and B. Hellström. Collector test method under quasi-dynamic conditions according to the european standard en 12975-2. *Solar Energy*, 76(1-3):117–123, 2004. ISSN 0038092x. doi: 10.1016/j.solener.2003.07.021.

N. Friling, M. J. Jiménez, H. Bloem, and H. Madsen. Modelling the heat dynamics of building integrated and ventilated photovoltaic modules. *Energy and Buildings*, 41(10):1051–1057, 2009. ISSN 03787788.

N. R. Kristensen and H. Madsen. Continuous time stochastic modelling, CTSM 2.3 - mathematics guide. Technical report, DTU, 2003.

N. R. Kristensen, H. Madsen, and S. B. Jørgensen. Parameter estimation in stochastic grey-box models. *Automatica*, 40 (2):225 – 237, 2004. ISSN 0005-1098. doi: DOI:10.1016/j.automatica.2003.10.001.

H. Madsen. *Time Series Analysis*. Chapman & Hall, 2007.

H. Madsen and J. Holst. Estimation of continuous-time models for the heat dynamics of a building. *Energy and Buildings*, 22(1):67–79, 1995. ISSN 03787788.

B. Perers. Dynamic method for solar collector array testing and evaluation with standard database and simulation programs. *Solar Energy*, 50(6):517–526, 1993. ISSN 0038092x.

B. Perers. An improved dynamic solar collector test method for determination of non-linear optical and thermal characteristics with multiple regression. *Solar Energy*, 59(4-6):163–178, 1997. ISSN 0038092x.

Solar Keymark. Homepage and database (all tested collectors according to EN12975 in Europe), 2011. URL `http://solarkey.dk/solarkeymarkdata/qCollectorCertificates/ShowQCollectorCertificatesTable.aspx`.